A novel function for Cyclin A2: Control of cell invasion via RhoA signaling

Nikola Arsic,[1,3,4] Nawal Bendris,[1,3,4] Marion Peter,[1,3,4] Christina Begon-Pescia,[1,3,4] Cosette Rebouissou,[1,3,4] Gilles Gadéa,[2] Nathalie Bouquier,[2] Frédéric Bibeau,[5] Bénédicte Lemmers,[1,3,4] and Jean Marie Blanchard[1,3,4]

[1]Institut de Génétique Moléculaire de Montpellier, and [2]Centre de Recherche en Biochimie Macromoléculaire, Centre National de la Recherche Scientifique, 34293 Montpellier, France
[3]Université Montpellier 2, 34095 Montpellier, France
[4]Université Montpellier 1, 34967 Montpellier, France
[5]Centre Régional de Lutte contre le Cancer Val d'Aurelle-Paul Lamarque, 34298 Montpellier, France

Cyclin A2 plays a key role in cell cycle regulation. It is essential in embryonic cells and in the hematopoietic lineage yet dispensable in fibroblasts. In this paper, we demonstrate that Cyclin A2–depleted cells display a cortical distribution of actin filaments and increased migration. These defects are rescued by restoration of wild-type Cyclin A2, which directly interacts with RhoA, or by a Cyclin A2 mutant unable to associate with Cdk. In vitro, Cyclin A2 potentiates the exchange activity of a RhoA-specific guanine nucleotide exchange factor. Consistent with this, Cyclin A2 depletion enhances migration of fibroblasts and invasiveness of transformed cells via down-regulation of RhoA activity. Moreover, Cyclin A2 expression is lower in metastases relative to primary colon adenocarcinoma in matched human tumors. All together, these data show that Cyclin A2 negatively controls cell motility by promoting RhoA activation, thus demonstrating a novel Cyclin A2 function in cytoskeletal rearrangements and cell migration.

Introduction

Cyclins govern progression through the cell cycle via their interactions with Cdks (Nigg, 1995; Morgan, 1997). Cyclin A2 controls both S phase and G2/M transition in association with Cdk2 and Cdk1, respectively (Pagano et al., 1992). During S phase, Cyclin A2 regulates the initiation and progression of DNA synthesis (Yam et al., 2002). At the G2/M transition, Cyclin A2 plays a critical role as a trigger for Cyclin B1–Cdk1 activation (Fung et al., 2007; De Boer et al., 2008). Cyclin A2 is essential for mouse embryonic development, and its conditional, postembryonic deletion reveals its requirement for establishment of the hematopoietic lineage (Murphy et al., 1997; Kalaszczynska et al., 2009).

Several observations indicate that Cyclins have kinase-independent functions. A kinase-dead Cyclin A–Cdk1 complex can still inhibit S phase in *Drosophila melanogaster* (Hayashi and Yamaguchi, 1999). A Cyclin E mutant that cannot activate Cdk2 still cooperated with activated Ras to transform cultured cells and was able to rescue the correct loading of minichromosome maintenance prereplicative complexes (Geisen and Moroy, 2002; Geng et al., 2007). Moreover, a computational analysis has suggested that the transcription factor C/EBP-β/NF-IL6 mediates the consequences of Cyclin D1 overexpression in some tumor samples in a Cdk4- or Cdk6-independent manner (Lamb et al., 2003). More recently, a proteomic screen revealed that several members of a network of DNA repair proteins interact with this Cyclin (Jirawatnotai et al., 2011)

Interestingly enough, Cyclin D1 has also been implicated in the control of cell motility through the Cdk inhibitor p27. Cyclin D1 sequestered p27, which led to increased cell motility (Li et al., 2006a,b,c). These and other studies indicate that Cyclin D1 and Cdk inhibitors, such as p21, p27, and p57, are important regulators of the Rho–Rho-activated kinase (ROCK)

N. Arsic and N. Bendris contributed equally to this paper.

Correspondence to Jean Marie Blanchard: jean-marie.blanchard@igmm.cnrs.fr; or Bénédicte Lemmers: benedicte.lemmers@igmm.cnrs.fr

Abbreviations used in this paper: Dbl, diffuse B-lymphoma; GAP, GTPase-activating protein; GAPDH, glyceraldehyde 3-phosphate dehydrogenase; GEF, guanine nucleotide exchange factor; Mant, *N*-methylanthraniloyl; NES, nuclear export signal; ROCK, Rho-activated kinase; shRNA, small hairpin RNA; WT, wild type.

The Rockefeller University Press $30.00
J. Cell Biol. Vol. 196 No. 1 147–162
www.jcb.org/cgi/doi/10.1083/jcb.201102085

signaling pathway that mediates cytoskeleton reorganization and cell motility (McAllister et al., 2003; Besson et al., 2004; Li et al., 2006c). The Rho family members RhoA, Rac1, and Cdc42 are small GTPases that regulate cell morphology, cytokinesis, and cell motility mainly through reorganization of Actin filaments. Rac1 controls the formation of lamellipodia, whereas Cdc42 triggers formation of filopodia and regulates cell polarity (Ridley et al., 1992; Etienne-Manneville and Hall, 2002; Vega et al., 2011). RhoA controls the assembly of Actin stress fibers and focal adhesions through Diaphanous and ROCK, which in turn regulates cytoskeletal proteins, such as Cofilin and Myosin light chain kinase (Ridley and Hall, 1992). Rho GTPase functions are tightly regulated, and their unbalanced activation can hinder cell migration (Ren et al., 2000; Schmidt and Hall, 2002; Vial et al., 2003; Heasman and Ridley, 2008). Guanine nucleotide exchange factors (GEFs) promote the exchange of GDP for GTP, hence activating Rho family proteins, whereas GTPase-activating proteins (GAPs) accelerate GTP hydrolysis, returning them to the inactive, GDP-bound state (Schmidt and Hall, 2002; Bos et al., 2007).

Our aim was to explore novel functions of Cyclin A2. To this end, we have used RNAi to deplete Cyclin A2 in cultured cells, followed by expression of wild-type (WT) or mutant proteins in the hope of differentially rescuing the resulting phenotypes. Small hairpin RNA (shRNA)–mediated knockdown of Cyclin A2 led to two major defects. The first one, as expected from the literature, consisted of cells accumulating at the G2/M boundary of the cell cycle (Fung et al., 2007). The second one, totally unexpected, involved important morphological changes, notably, increased cell diameter and volume that reflect cytoskeleton modifications, in particular redistribution of Actin fibers and Vinculin. This novel role of Cyclin A2 was independent of Cdk binding, instead being mediated by its direct binding to RhoA and the regulation of its GTP loading. Consistent with this, depletion of Cyclin A2 impaired RhoA activation and resulted in increased cell motility and invasiveness, all of which were reversed by expression of WT Cyclin A2 or a mutant incapable of binding and activating Cdk. Moreover, analysis of matched samples of human colorectal primary tumors and their corresponding metastases showed a strong decrease in Cyclin A2 levels in the latter, which implies a key regulatory role for Cyclin A2 in limiting cell invasiveness in vivo.

Results

Depletion of Cyclin A2 delays entry into mitosis and induces cell morphology alterations

We checked five different shRNAs (shRNA a–e; see Materials and methods) that target Cyclin A2 in NIH3T3 cells; two of them (shCycA2-a and -b) led to ≥80% extinction of Cyclin A2 (Fig. 1 A and Fig. S1 A). They were both used throughout this work except in human cells, in which only shCycA2-b, targeting a conserved sequence, led to efficient depletion.

Because both gave the same results in all experiments, we present the data obtained with shRNA b except for the rescue experiments (see Fig. 2 D, Fig. 3 A, and Fig. 5 C) in which shRNA a was used. The same vector expressing an shRNA directed against firefly luciferase (shLuc) was used as a control. Confluent cells were reseeded and analyzed by FACS 24 h later. The shCycA2-infected cells show an accumulation in G2/M, most likely reflecting the delayed entry into mitosis previously reported by others (Fig. 1 B and Fig. S1 C; Fung et al., 2007). Nevertheless, these cells continue to proliferate, albeit at a lower pace (Fig. S1 D), and presented increased p21 levels but almost no detectable p27 (Fig. S1 E).

Surprisingly, Cyclin A2–depleted cells show an increase in cell size relative to control cells as detected by microscopy and by direct monitoring of cell parameters in adherent conditions (Fig. S2) as well as in suspension (Fig. S1, F and G). More than 80% of the cells exhibited an isotropic increase in size (Fig. S1, F and G; and Fig. S2, B–G) and protrusions, whereas a small proportion had an elongated phenotype or a rounded nestlike phenotype (Fig. S2 A). We investigated whether this reflected an alteration in the Actin cytoskeleton, which was visualized by staining cells with phalloidin. Although control cells showed cytoplasmic bundles of Actin fibers as expected (Fig. 1 C, top), these were strongly reduced in shCycA2-treated cells, which instead showed cortical localization of F-Actin (Fig. 1 C, bottom). This was associated with a redistribution of focal adhesion complexes visualized by Vinculin staining (Fig. 1 C). Notably, immunoblots demonstrated that the total amount of Vinculin remained unchanged (unpublished data). These alterations have been observed in several cell types (Fig. S3).

Because Cyclin A2–depleted cells accumulated in G2/M, we checked whether the Actin cortical distribution was simply a consequence of this cell cycle bias. Therefore, NIH3T3 cells were blocked at the G2/M boundary by treatment with RO 3306, an inhibitor of Cdk1 (Fig. 1 D; Vassilev, 2006). Nevertheless, they showed the same cytoplasmic-wide distribution of Actin fibers observed in control DMSO-treated cells and no disruption of focal adhesions (Fig. 1 E). This indicated that this phenotype was caused by the absence of Cyclin A2.

To rule out off-target effects, we reintroduced vectors expressing WT and mutant (Mut) versions of Cyclin A2 that are resistant to shCycA2 (Fig. 2 A). Mut1–Cyclin A2 contains a single amino acid change (D171A) that impaired Cyclin A2 binding to Cdk2 in *Xenopus laevis* (Goda et al., 2001) but is fully active in mouse cells (Fig. 2 B). In contrast, Mut2–Cyclin A2, which contains three amino acids changes (M200A, L204A, and W207A) in the Cyclin box (Schulman et al., 1998), was compromised in its ability to interact with Cdk1 and Cdk2, as well as other partners, such as p21, p27, or p107. Consequently, this mutant was not associated with any histone H1 kinase activity (Fig. 2, A and B). Expression of shRNA-resistant WT Cyclin A2 restored a normal cell cycle distribution, unlike Mut2–Cyclin A2 (Fig. 2 C).

With regards to the Actin phenotype, expression of shRNA-resistant WT Cyclin A2 in Cyclin A2–deficient cells restored the normal cytoplasmic distribution of Actin. Surprisingly, expression of shRNA-resistant Mut2–Cyclin A2 had the same effect (Fig. 2 D). Cyclin A2 contains no NLS and shuttles between the cytoplasm and the nucleus because of its binding partners (Jackman et al., 2002). This could explain the cytoplasmic

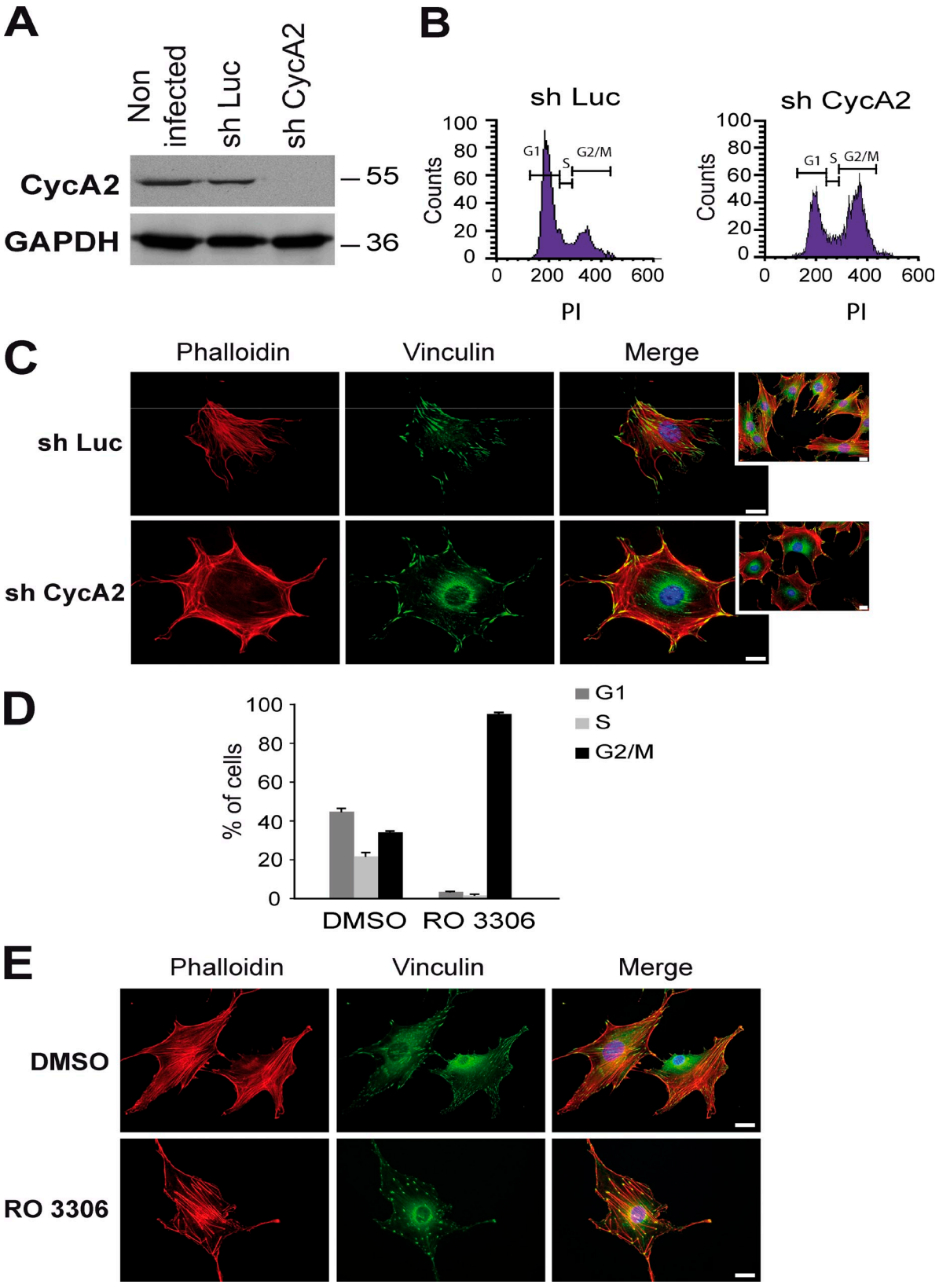

Figure 1. **Depletion of Cyclin A2 in NIH3T3 cells induces an accumulation of the cells in G2/M and a reorganization of Actin cytoskeleton and focal adhesion distribution.** (A) Western blot analysis of Cyclin A2 depletion performed in noninfected, mock-infected cells (shLuc), or cells infected with a virus expressing an shRNA targeting Cyclin A2 (shCycA2). GAPDH is used as a loading control. Molecular markers are given in kilodaltons. (B) Cell cycle distribution of shLuc and shCycA2 NIH3T3 cells after release from a synchronization block. (C and E) Staining of F-Actin with phalloidin-rhodamine (red) and Vinculin (green) in NIH3T3 cells infected with shLuc or shCycA2 (C) or treated with the Cdk1 inhibitor RO 3306 or DMSO as a control (E). (insets) Fields with lower magnification. Bars, 20 µm. (D) FACS analysis of cell cycle distribution of NIH3T3 cells treated with RO 3306 (Cdk1 inhibitor) or DMSO as a control. Data are represented as means ± SEM (n = 3). PI, propidium iodide.

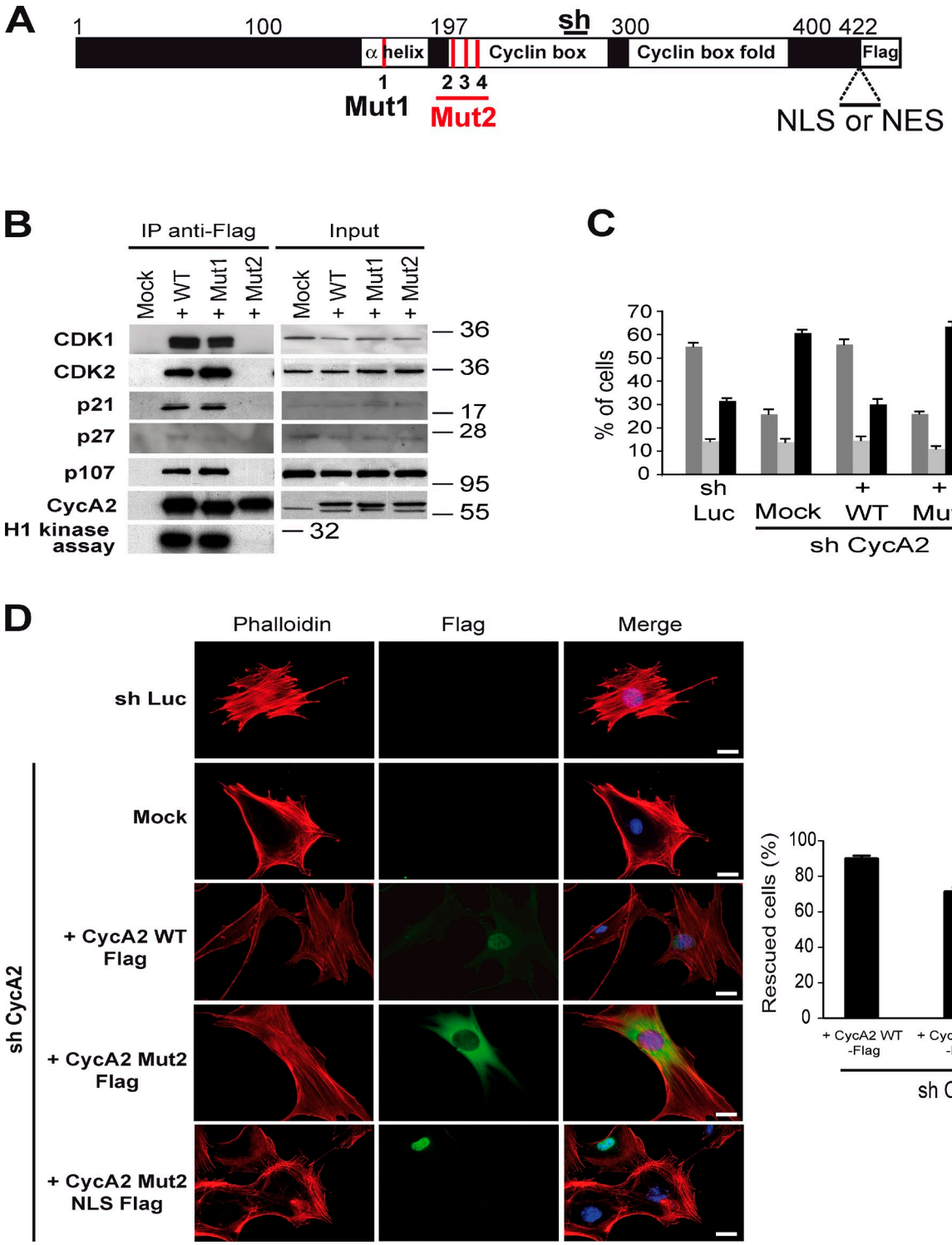

Figure 2. **Reintroduction of both WT and Mut2–Cyclin A2 reverses F-Actin corticalization induced by Cyclin A2 depletion.** (A) Schematic representation of mouse Cyclin A2 protein and modifications induced in this study. Mut1 and Mut2 show substitution of amino acid residues N171 or M200, L204, and W207, respectively, into alanines by site-directed mutagenesis. All constructs were C-terminally fused to three Flag tags. When required, nuclear localization (NLS) or nuclear export (NES) signals were introduced between the Cyclin A2 coding sequence and the Flag tags. The position of the shRNA sequence leading to undetectable levels of Cyclin A2 is indicated. (B) Analysis of binding and kinase-activating properties of Cyclin A2 mutants. Immunoprecipitation (IP) using anti-Flag–agarose affinity gel was performed on NIH3T3 cells extracts after transfection by WT–, Mut1–, or Mut2–Cyclin A2. Immune complexes were either submitted to Western blotting to identify binding partners or analyzed for their histone H1 kinase activity. Molecular markers are given in kilodaltons. (C) Cell cycle distribution of control and Cyclin A2–deficient cells infected with virus expressing wild-type (WT) and mutant Cyclin A2 (Mut2). Synchronized cells were analyzed 24 h after release from the proliferation block. Data are represented as means ± SEM (n = 3). (D) Immunofluorescence analysis of F-Actin organization of shCycA2 NIH3T3 cells transfected with plasmids encoding WT, Mut2, or Mut2 with NLS (Mut2-NLS) Cyclin A2 fused to a Flag tag. F-Actin was stained as in Fig. 1. Transfected Cyclin A2 proteins were detected with the anti-Flag antibody. Bars, 20 µm. The graph refers to the percentage of transfected cells harboring a reversion of the cortical phenotype (150–200 cells were scored for each case). Data are represented as means ± SEM (**, P = 0.0056; n = 4).

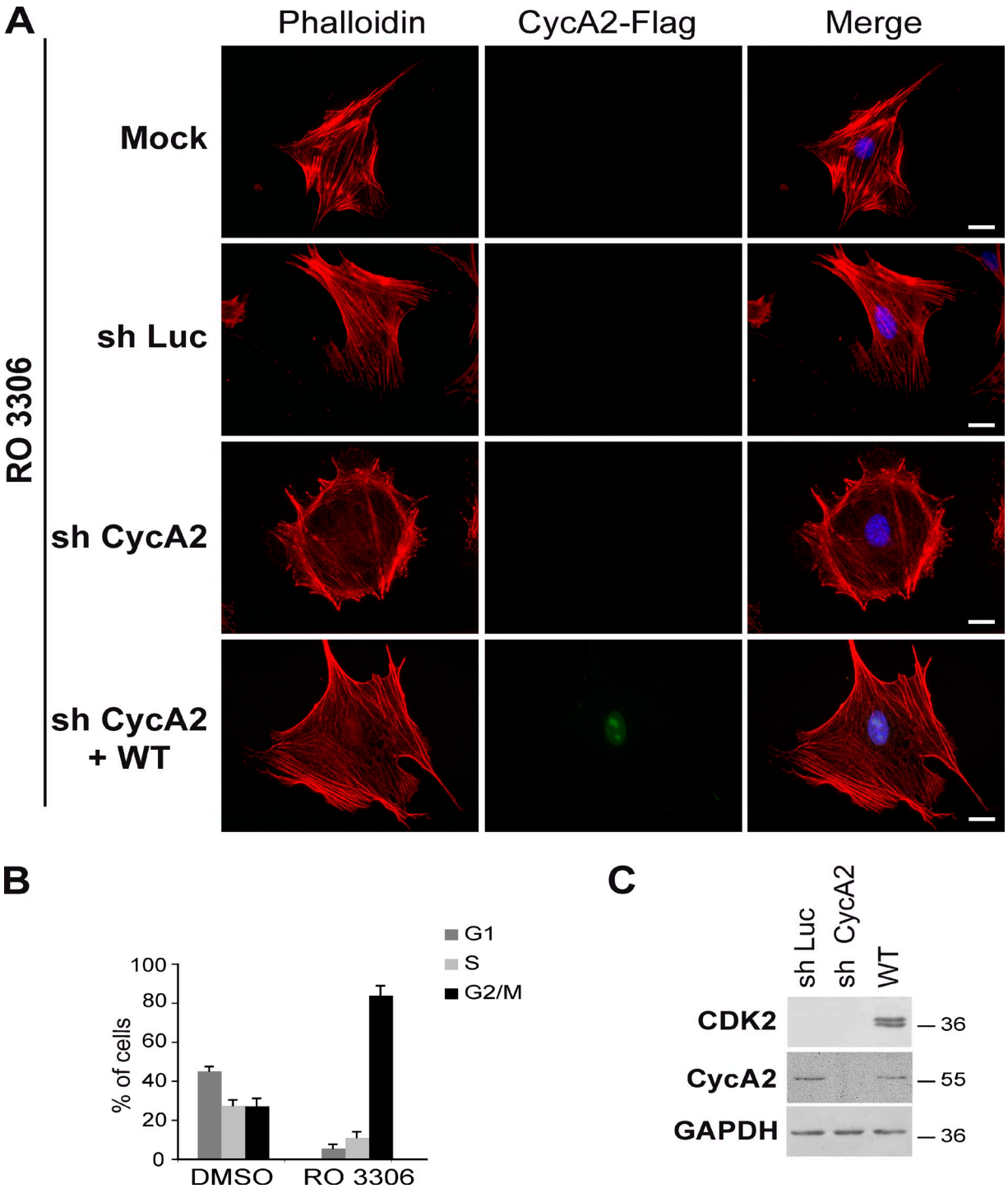

Figure 3. **Rearrangement of Actin cytoskeleton upon Cyclin A2 depletion is independent of Cdk1 and Cdk2 activities.** (A) F-Actin (red) and Cyclin A2 (green) staining by phalloidin or anti-Flag antibody of *Cdk2*$^{-/-}$ cells treated with the Cdk1 inhibitor RO 3306. *Cdk2*$^{-/-}$ cells were infected with CycA2 shRNA and transfected with wild-type (WT) Cyclin A2. Bars, 20 µm. (B) FACS analysis of cell cycle distribution after treatment of *Cdk2*$^{-/-}$ cells with RO 3306 for 24 h. Data are represented as means ± SEM (n = 3). (C) Western blot analysis of Cdk2 and Cyclin A2 after infection with CycA2 shRNA in *Cdk2*$^{-/-}$ cells. GAPDH is used as a loading control. Molecular markers are given in kilodaltons.

localization of the mutant, which cannot bind to either Cdk or other Cyclin A2 partners (p21, p27, and p107). We therefore wondered whether forcing its nuclear localization via fusion to the SV40 NLS would affect its ability to restore a normal Actin cytoskeleton. Indeed, cells expressing nuclear-localized Mut2–Cyclin A2 (Mut2-NLS) showed the cortical Actin cytoskeleton phenotype (Fig. 2 D), i.e., in this situation the mutant was unable to correct for Cyclin A2 depletion. Some cells, expressing high levels of Mut2-NLS, displayed both nuclear and cytoplasmic localization; importantly, they showed a normal distribution of the Actin cytoskeleton and Vinculin (unpublished data). Consistent with this, WT Cyclin A2 fused to a potent nuclear

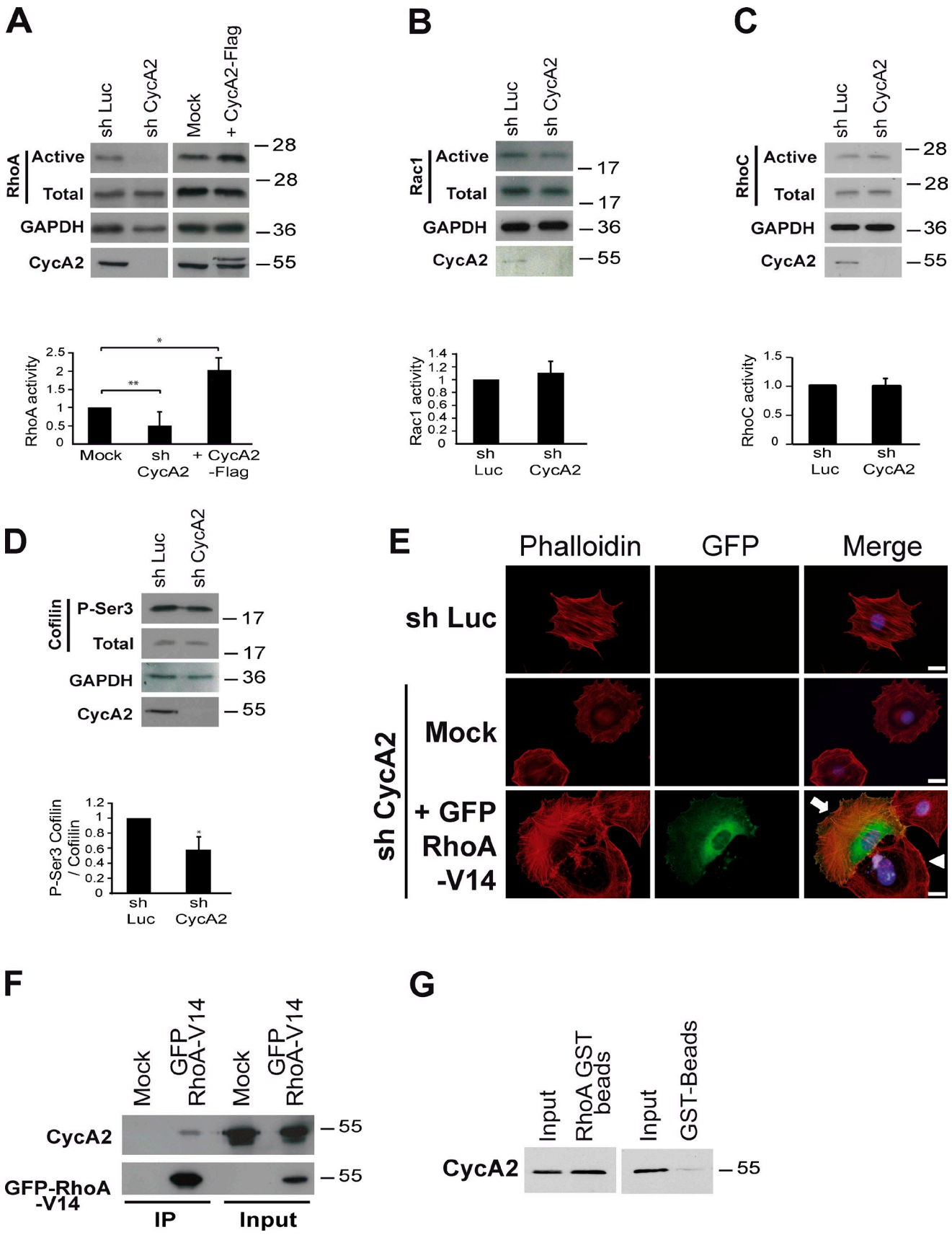

Figure 4. **Cyclin A2 directly interacts with RhoA and regulates its activation state.** (A–C, top) Western blotting after pull-down of activated forms of RhoA (A), Rac1 (B), or RhoC (C) after depletion (A, left–C) or forced expression (A, right) of Cyclin A2. (bottom) Corresponding quantifications from independent pull-down experiments (normalization of the GTP-bound forms to total RhoA, Rac1, or RhoC and GAPDH). Data are represented as means ± SEM (*, P = 0.031;

export signal (NES) was also able to correct the phenotype, even when NES–Cyclin A2 was predominantly cytoplasmic (unpublished data).

To definitively rule out any role for Cdk in the aforementioned observations, we performed the rescue in a Cdk1/Cdk2-deficient context. The early lethality of *cdk1*$^{-/-}$ embryos makes it impossible to derive Cdk1-deficient cells (Martín et al., 2005); therefore, we used the Cdk1 inhibitor RO 3366 in Cdk$^{-/-}$ mouse fibroblasts (Fig. 3 B). As with WT cells, shRNA-mediated depletion of Cyclin A2 under these conditions (Fig. 3 C) led again to a cortical distribution of Actin that returned to normal upon reexpression of WT Cyclin A2 (Fig. 3 A). These data reveal a novel function for Cyclin A2 in the cytoplasm that requires neither association with nor activation of Cdk1 and Cdk2.

Cyclin A2 down-regulation affects RhoA activity

Rho GTPases control several cytoplasmic processes, including Actin dynamics, membrane protrusion, and thereby, cell migration (Etienne-Manneville and Hall, 2002; Sahai and Marshall, 2002; Heasman and Ridley, 2008; Vega and Ridley, 2008). Given this and the aforementioned data, we analyzed RhoA, RhoB, RhoC, and Rac1 activity in Cyclin A2–depleted cells using a GTP-bound GTPase pull-down assay. Cell extracts were incubated with either GST-Pak1–p21-binding domain for Rac1 or GST-Rhotekin–Rho-binding domain for RhoA, RhoB, and RhoC, and the bound proteins were visualized by immunoblotting. Although RhoB was barely detectable (Fig. S4 C), RhoA activity was decreased after depletion of Cyclin A2 compared with shLuc-treated cells (Fig. 4 A, left). In contrast, Rac1 and RhoC activities were unaffected (Fig. 4, B and C). Conversely, expression of WT Cyclin A2 resulted in increased RhoA activity (Fig. 4 A, right). Accordingly, Cofilin phosphorylation on Serine 3 was significantly decreased (46%) in Cyclin A2–deficient cells (Fig. 4 D); this change in its phosphorylation status could be caused by this or other signaling pathways regulating its activity.

The simplest explanation for this decrease in RhoA activity would be that Cyclin A2 depletion leads to the inhibition of a GEF or activation of a GAP. This was tested by expressing a constitutively active version of RhoA, namely GFP-RhoAV14, which is insensitive to such regulators, in Cyclin A2–deficient cells. GFP-positive cells lose the cortical distribution of F-Actin, which is now distributed throughout the cytoplasm (Fig. 4 E). Cells with a high expression level of the GTPase were much smaller than control cells and showed a more rounded, less spread morphology associated with dense cytoplasmic Actin bundles (unpublished data). These data demonstrate that the absence of Cyclin A2 leads to a decrease in the GTP-bound fraction of RhoA that could result from an alteration of the interactions of the GTPase with its regulators or by a direct effect of Cyclin A2 on GAP or GEF activities toward RhoA.

We then tested whether Cyclin A2 could be found in a complex with RhoA. To address this possibility, we expressed GFP-tagged RhoA (Fig. 4 F) and immunopurified complexes from cell lysates. Immunoblot analysis of the complexes showed that ectopic RhoA copurified with endogenous Cyclin A2 (Fig. 4 F). Interestingly, although Cyclin A2 was able to interact with all forms of RhoA, we reproducibly noticed that both RhoAWT and its dominant-negative form RhoAN19 bound to a faster migrating form of the cyclin (Fig. S4 A). This suggests that RhoAWT and N19 are interacting with either a Cyclin A2 cleaved form, previously observed in stem cells and myeloid precursors (Welm et al., 2002; Kalaszczynska et al., 2009), or with a Cyclin A2 form subject to posttranslational modifications. Further studies on this are currently in progress.

To establish whether their interaction was direct, both proteins were purified after expression in bacteria. Indeed, recombinant Cyclin A2 bound to GST-RhoA immobilized on glutathione–agarose beads (Fig. 4 G).

We used vectors expressing either the N-terminal 196 amino acids of Cyclin A2 or the remaining C-terminal portion, which contains the Cyclin box domain, to further localize the motif involved in both RhoA binding and restoration of cytoplasmic Actin distribution (Fig. 5 A). The Cyclin A2 N-terminal domain strongly interacted with RhoA and restored the normal cytoplasmic distribution of Actin, activities not observed with the C-terminal region (Fig. 5, B and C). These data support a model in which Cyclin A2, through its N-terminal domain, interacts directly with and modulates the activity of RhoA. Notably, this is independent of Cdk1 and Cdk2.

We next assayed whether the loading state of RhoA affected the affinity of Cyclin A2 for the GTPase. Fig. 6 A shows that Cyclin A2 binds more avidly to nucleotide-free RhoA than to both RhoA-GTP or RhoA-GDP. Nucleotide-free RhoA is a transient form during the GTPase activation process. We thus resorted to an in vitro *N*-methylanthraniloyl (Mant)-GTP kinetic fluorescence assay to address the potential of Cyclin A2 to modulate the exchange activity of diffuse B-lymphoma (Dbl), a RhoA-specific GEF (Yoshizuka et al., 2004). Similar results were obtained with another GEF: Tgat (Trio-related transforming gene in adult T cell leukemia/lymphoma tumor cells), an oncogenic splicing isoform of the Rho GEF Trio. When added to the assay, Cyclin A2 led to a 40% increase in the initial exchange velocity of the GEFs (Fig. 6, B–E), which was not the

**, P = 0.003; *n* = 5 for shCycA2, *n* = 3 for CycA2-Flag for the RhoA pull-down assay, and *n* = 3 for the Rac1 and RhoC pull-down assays). (D) Western blot analysis (top) and quantification (bottom) of the phosphorylation state of the RhoA–ROCK effector Cofilin (±SEM; *, P = 0.031; *n* = 3). (E) Detection of the rescue of cytoskeleton corticalization by constitutively active RhoA (green) in Cyclin A2–depleted cells using F-Actin staining (red). The arrow points to a RhoA-expressing cell, and the arrowhead points to a nontransfected cell. Bars, 20 µm (F) Coimmunoprecipitation (IP) of endogenous Cyclin A2 with RhoA. Cell lysates obtained from NIH3T3 cells transfected with RhoAV14-GFP were immunoprecipitated by GFP-Trap beads. Interaction between the two molecules was detected after blotting with an anti–Cyclin A2 antibody after GFP pull-down. (G) Cyclin A2 directly interacts with RhoA. Recombinant Cyclin A2 was incubated either with glutathione beads as control or RhoA-GST bound to glutathione beads. Cyclin A2 bound to RhoA-GST was detected by Western blotting after elution. Molecular markers are given in kilodaltons.

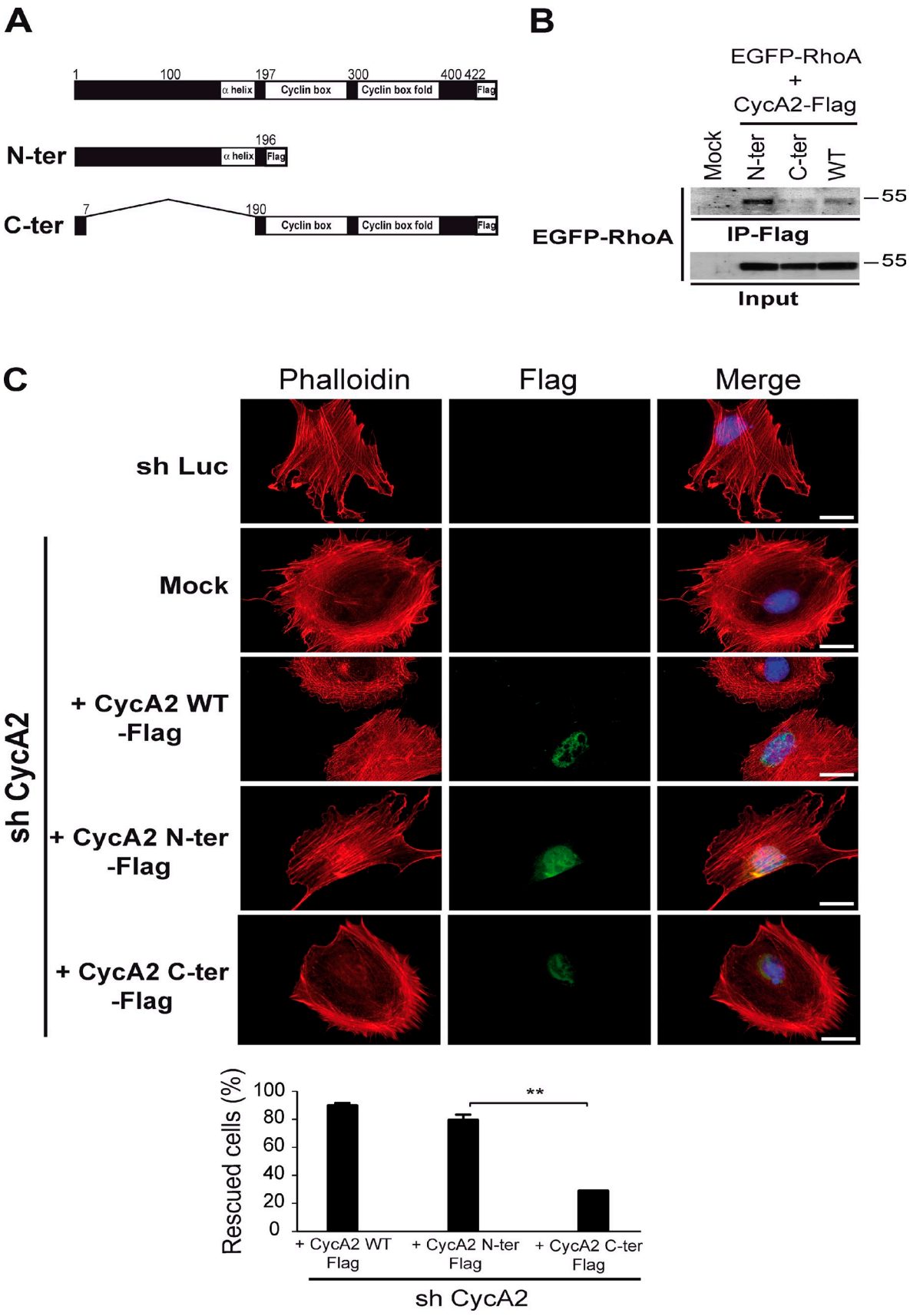

Figure 5. **The N-terminal domain of Cyclin A2 mediates its interaction with RhoA and restores cytoplasmic bundles in Cyclin A2–deficient cells.** (A) Schematic representation of Cyclin A2 deletion mutants. The first one encompasses the N-terminal part of Cyclin A2 upstream of the Cyclin box (N-ter). The second contains the C-terminal part of the protein including the Cyclin box (C-ter). The latter construct contains amino acids 1–7, allowing proper expression of

case for irrelevant proteins, such as GST or MBP (maltose-binding protein). Moreover, when introduced in the same assay, only the N-terminal half of Cyclin A2 led to an increased GEF-promoted exchange activity, whereas the C-terminal Cyclin A2 half or Cyclin E1 not only did not potentiate this activity but even restrained it (Fig. 6, F and G). Collectively, this suggests that Cyclin A2, through its binding to RhoA, potentiates GDP-GTP exchange activity of the Rho GEF and thus promotes an active RhoA state.

Cyclin A2–depleted cells display increased motility

Decreases in the number of focal adhesions and in Cofilin phosphorylation are often associated with diminished cell adhesion and increased motility (Oser and Condeelis, 2009). Given the aforementioned data, we analyzed both parameters in shLuc- versus shCycA2-treated cells. After replating, Cyclin A2–deficient cells showed a twofold drop in adherence to culture dishes (Fig. S1 H). In wound-healing assays, Cyclin A2–deficient cells were more motile than control cells (Fig. 7 A) as quantified using time-lapse video microscopy (Video 1 and Video 2). Cells lacking Cyclin A2 showed a 55% increase in area coverage compared with control cells. This increase was reversed, i.e., cells returned to the control migration rate, upon expression of shRNA-resistant WT or Mut2–Cyclin A2 (Fig. S5). The same results were obtained when migration was assayed in Boyden chambers (Fig. 7 B).

We then assessed cell invasion in a 3D collagen I matrix (Smith et al., 2008). Control NIH3T3 cells were not motile, and knockdown of Cyclin A2 had little effect on promoting their invasive properties in this assay (Fig. 7 C). Because transformation is often necessary to acquire 3D invasive properties in these cells, we performed the experiment using NIH3T3 cells transformed with RasV12. Indeed, this strongly enhanced the invasiveness of the control shLuc-expressing cells, and importantly, depletion of Cyclin A2 doubled their invasive capacity (Fig. 7 C). These data demonstrate that Cyclin A2–deficient cells are more motile than their WT counterpart in a 2D migration assay. Moreover, in a 3D invasion test, loss of Cyclin A2 increases invasiveness in cells transformed by oncogenic Ras.

Cyclin A2 in human transformed cells and samples from matched tumors

These observations led us to evaluate the effect of Cyclin A2 depletion in human cancer-derived cell lines, such as MDA-MB-231, classically used in invasion assays. Again, shRNA-mediated Cyclin A2 knockdown in these cells led to a twofold increase in their ability to invade the collagen matrix (Fig. 7 D). Conversely, overexpression of WT Cyclin A2 significantly diminished invasiveness relative to the control cells (Fig. 7 D). These data suggest that, in transformed cells, decreased levels of Cyclin A2 might be linked to metastasis. To confirm this idea, we measured Cyclin A2 levels in SW480 and SW620 cells, which were derived from a primary colon carcinoma (SW480) and a distant lymph node metastasis (SW620) in the same patient (Leibovitz et al., 1976). SW620 cells show increased invasive potential in the Boyden chamber assay (Bergmann-Leitner and Abrams, 2000). Consistent with our idea, SW620 cells express Cyclin A2 at 40% the level seen in SW480 cells (Fig. 8 A).

We felt it was essential to substantiate these observations in samples from human primary tumors. Therefore, we used immunoblotting to measure Cyclin A2 levels in crude extracts prepared from 12 sets of matched tumor samples obtained via biopsies of primary colorectal adenocarcinomas and their corresponding metastases. Glyceraldehyde 3-phosphate dehydrogenase (GAPDH) immunoreactivity showed relatively similar protein loading in each lane (Fig. 8 B). Interestingly, the Cyclin A2 signal was systematically and significantly higher in primary tumor samples relative to their metastatic counterparts (Fig. 8 B). We completed this analysis by an immunohistochemical survey of a tissue array. Cyclin A2 expression was restricted to the proliferating normal cells of the intestinal crypts and to the tumoral tissue. There was no contribution of stromal cells. A representative staining is shown in Fig. 8 C for three different matched samples and confirms the lower amount of Cyclin A2 in metastases versus primary tumors. Notably, some tumor cells show the presence of Cyclin A2 in the cytoplasm (Fig. 8 C, inset) as already described for renal cell carcinoma (Aaltomaa et al., 1999). This confirms and strengthens the conclusion drawn from cultured cell lines and demonstrates that, in vivo, decreased Cyclin A2 expression occurs during metastasis.

Discussion

Our aim was to investigate alternative functions for Cyclin A2. To accomplish this, we performed a knockdown of Cyclin A2 expression in a variety of cell lines. In all cases, cells lacking Cyclin A2 were able to proliferate, although they accumulated in G2/M, which likely reflects their delayed entry into mitosis.

Surprisingly, Cyclin A2–deficient cells contain a perturbed cytoskeleton, in which Actin filaments are cortical, and the distribution of focal adhesions is altered. This corresponded to the down-regulation of the RhoA–ROCK pathway and decreased phosphorylation of Cofilin, which is involved in the reorganization of Actin filaments (Moriyama and Yahara, 1999), consecutively leading to an increased cell migration and invasion. In contrast, Cyclin A2 overexpression increased the proportion of active RhoA and decreased invasive behavior in a 3D collagen matrix. Furthermore, our results suggest that regulation of RhoA

the protein. Flag tag was fused to the C-terminal part of each fragment. (B) Interaction of RhoA with Cyclin A2 fragments. Immunoprecipitations (IP) using anti-Flag–agarose affinity gel were performed on NIH3T3 cells cotransfected with plasmids encoding RhoA-EGFP and N-terminal, C-terminal, or full-length Cyclin A2. Binding of RhoA to the different fragments was detected by immunoblotting using anti-GFP antibodies. Molecular markers are given in kilodaltons. (C) Cyclin A2 fragments were expressed in Cyclin A2–deficient NIH3T3 cells and detected by immunofluorescence using anti-Flag antibody (green), whereas F-Actin was detected using phalloidin staining (red). Bars, 20 µm. Graph refers to the percentage of transfected cells harboring a reversion of the cortical phenotype. Data are represented as means ± SEM (**, P = 0.006; *n* = 3).

Figure 6. **Cyclin A2 potentiates RhoA GEF exchange activity.** (A) Interaction of Cyclin A2 with either nucleotide-free GST RhoA or GST RhoA loaded, respectively, with GDP or GTP (left) and quantification of retained Cyclin A2 (right). Molecular markers are given in kilodaltons. (B–G) Kinetics of Mant-GTP loading by Dbl (B) and Tgat (D). Results are expressed as fluorescence units versus time. The reactions performed in the absence of GEFs and with irrelevant proteins (MBP or GST) reflect the spontaneous exchange activity of RhoA. In F and G, the N- and C-terminal halves as well as Cyclin E1 are included in the assay. C, E, and G represent a normalized quantitative analysis of the initial velocity measured in six independent experiments (B and C) and three independent experiments (D–G). Data are represented as means ± SEM (*, P = 0.03; **, P = 0.0081). WB, Western blot; N-ter, N-terminal; C-ter, C-terminal.

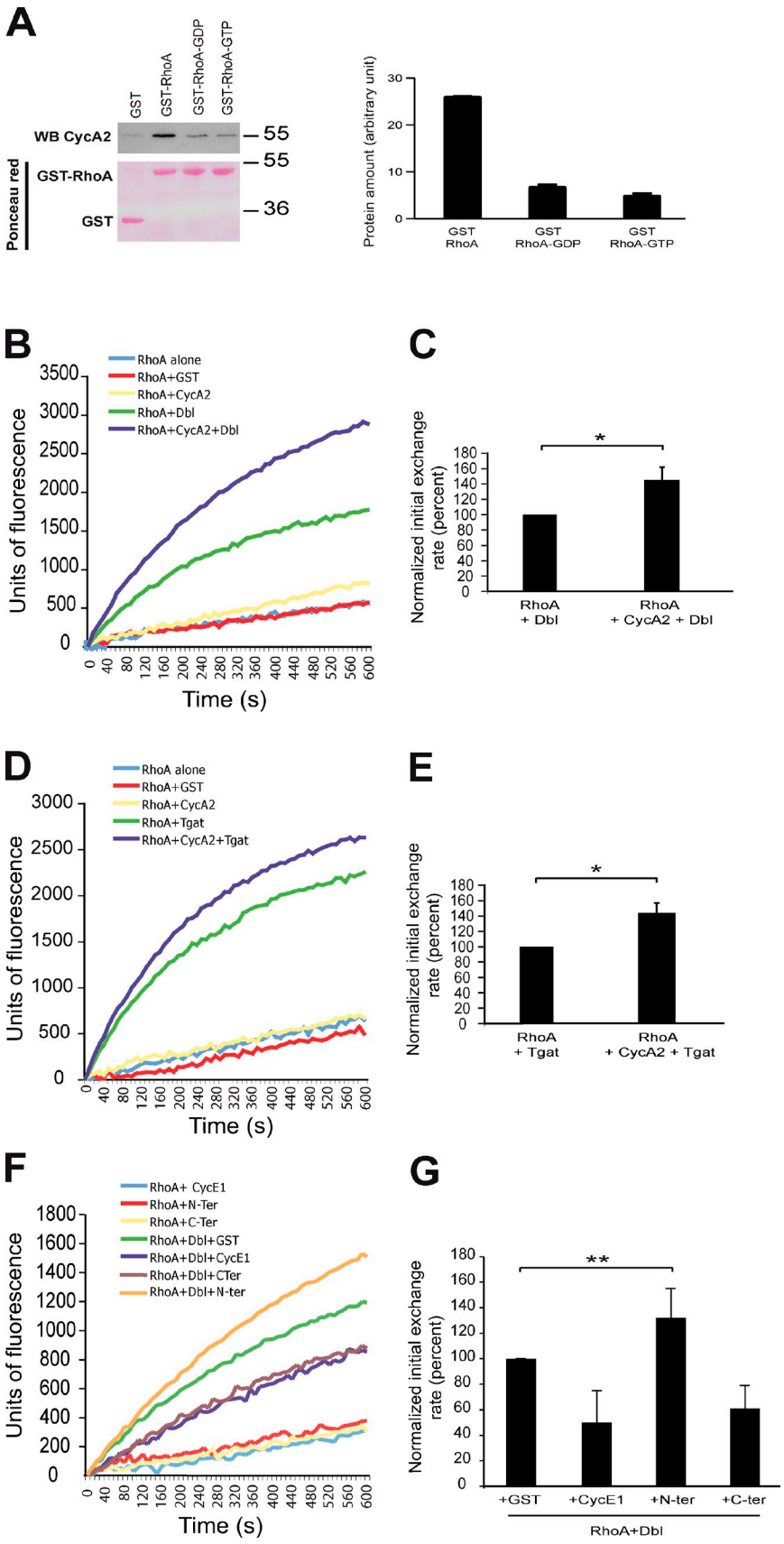

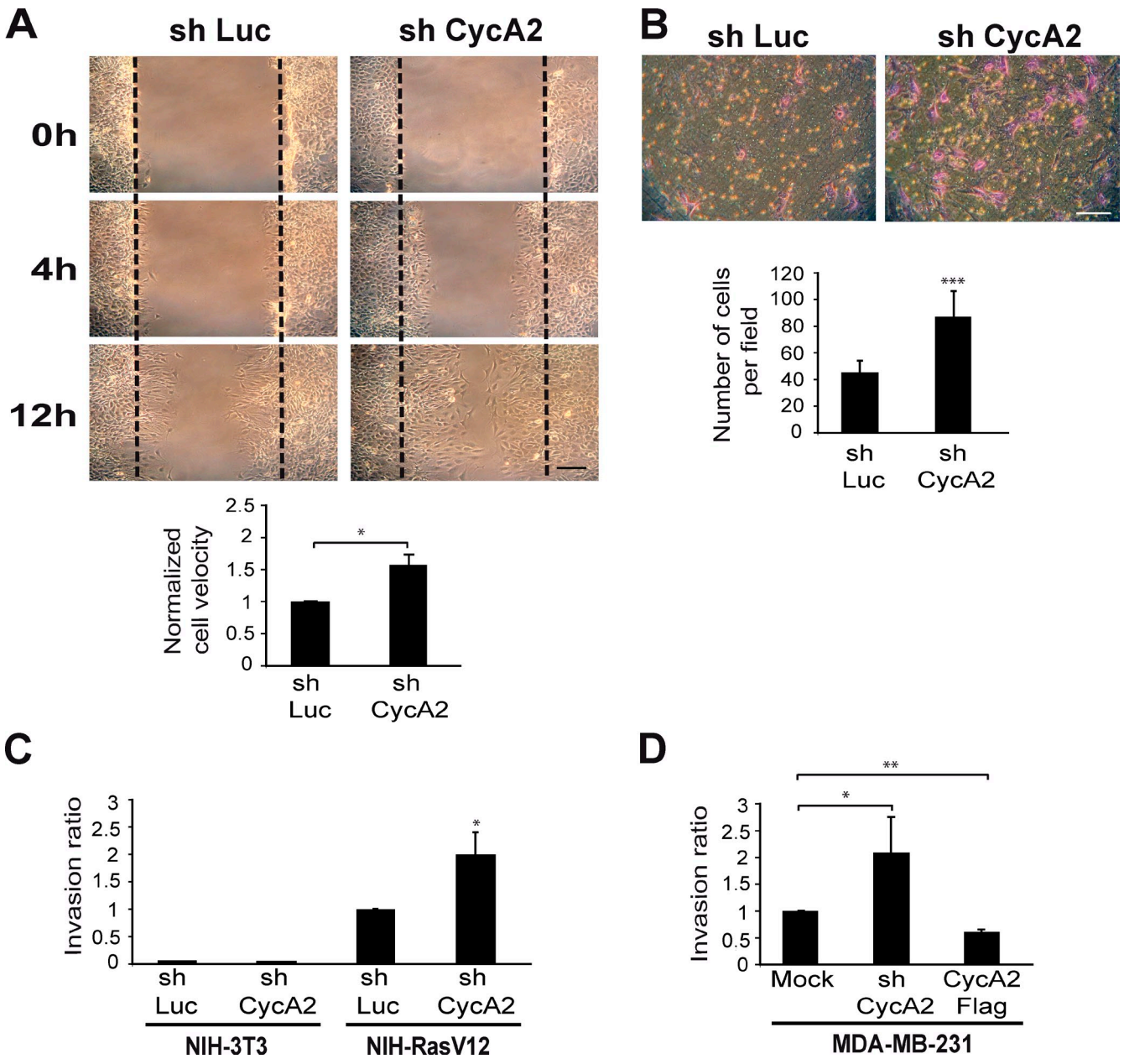

Figure 7. **Cyclin A2 modulates cell migration and invasion.** (A) Wound-healing migration assay performed on confluent NIH3T3 cells infected with shLuc or shCycA2. Pictures were taken at the time of scratch (t = 0) and 4 and 12 h afterward. Migration velocities were calculated after time-lapse acquisitions for 22 h and normalized with shLuc condition. (*, P > 0.05; *n* = 3). Black dotted lines indicate scratch limits. Bar, 200 µm. (B) Representative microscope fields of insert membranes after a Boyden chamber migration assay and quantification of the stained cells (P = 0.0007; *n* = 3). Bar, 100 µm. ***, P = 0.0001. (C and D) Cell invasion in 3D collagen matrix for NIH3T3 and NIH3T3-RasV12 cells (C; *, P = 0.01; *n* = 6) and MDA-MB-231 cells after depletion or forced expression of Cyclin A2 (D; *, P = 0.015; **, P = 0.0043; *n* = 6). Invasion ratios were relative to either shLuc-treated cells (C) or to cells infected with empty virus (D). Data are means ± SEM.

activity by Cyclin A2 could be mediated through their interaction, whereby Cyclin A2 acts as a platform promoting GEF exchange activity toward RhoA.

Consistent with their strong sequence similarity, the three Rho GTPases are able to interact with Cyclin A2, which is not the case for Rac1 (Fig. S4 B, D, and E). It remains to be established to which extent Cyclin A2 deregulation impacts their activities in other cellular contexts.

In fibroblasts, RhoA activation promotes the formation of stress fibers and focal adhesions, whereas active Rac1 is linked to their disassembly (Burridge and Wennerberg, 2004). Moreover, the two pathways show regulatory cross talk: activation of one results in inhibition of the other, the net outcome for a cell reflecting a balance between the two pathways (Burridge and Wennerberg, 2004). Strikingly, this balance is disrupted in Cyclin A2–depleted cells, in which diminished RhoA activity was uncoupled from that of Rac1.

Interestingly, Cyclin D1 and Cdk inhibitors p21 and p27 have additional functions that involve the RhoA–ROCK pathway. Cyclin D1 binds directly to p27 and thereby blocks

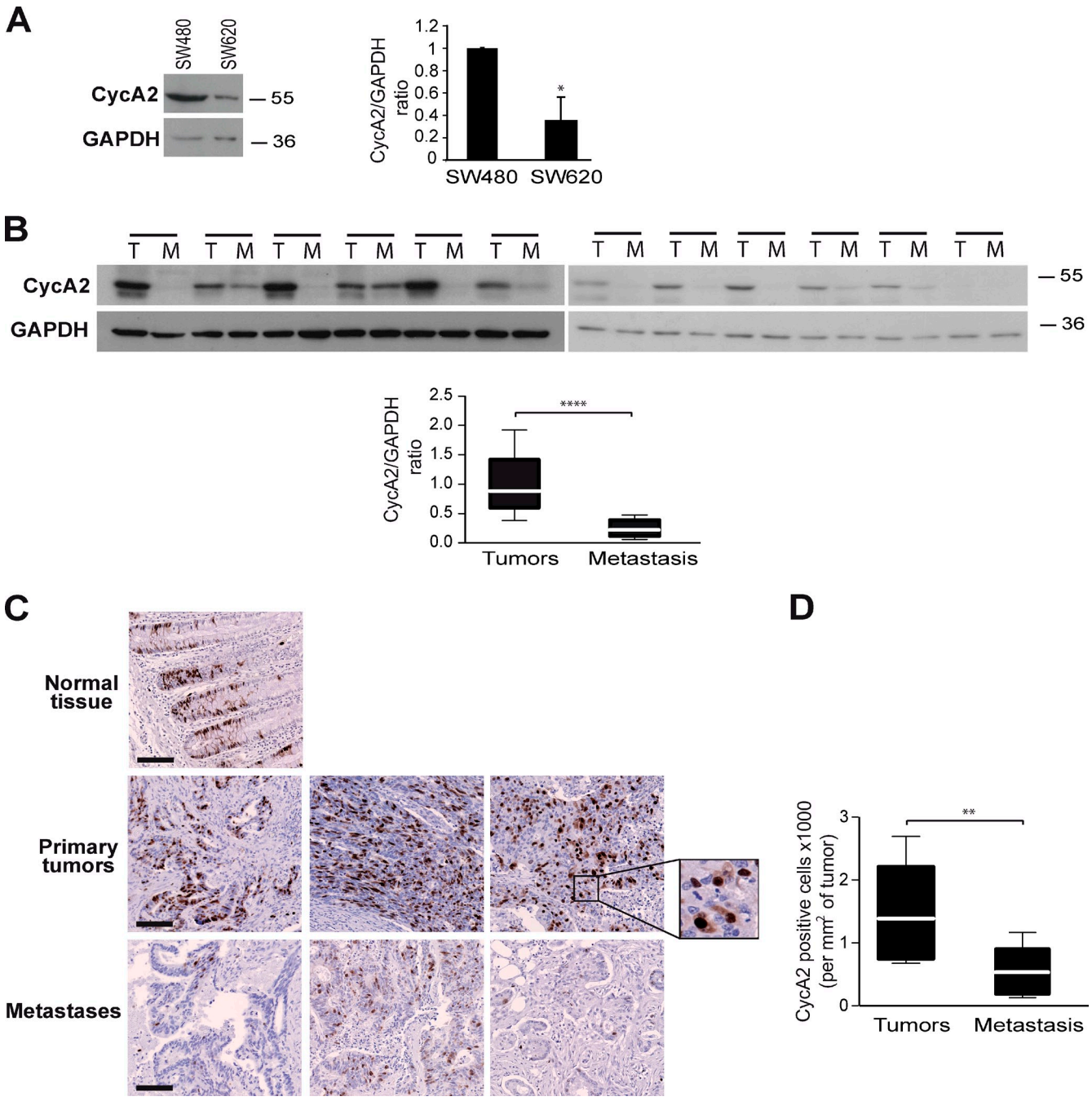

Figure 8. **Cyclin A2 is differentially expressed in primary human tumors versus metastases.** (A and B) Cyclin A2 quantification in SW480 and SW620 cells (A; *, P = 0.031) or matched human primary colorectal tumors (T) and their corresponding metastases (M) from 12 individuals (B; ****, P > 0.0001). Identical amounts of protein extracts were loaded. Data are means ± SEM. (C) Three representative examples of immunohistological Cyclin A2 staining in primary colorectal tumors (middle) and their metastases (bottom) versus normal tissue (top). (inset) Enlargement of the indicated region shows cytoplasmic Cyclin A2 staining. Bars, 100 µm. (D) Quantification was performed on eight matched samples (**, P = 0.0055). Molecular markers are given in kilodaltons. Bars (whiskers) represent maximum and minimum values; the white line corresponds to the median.

RhoA activation by inhibiting interaction with its GEF (Besson et al., 2004; Li et al., 2006a,b,c). Similarly, cytoplasmic p21 has been shown to bind and inhibit ROCK1, which promotes neurite extension by neuroblastoma cells and hippocampal neurons (Tanaka et al., 2002). In contrast, we show that Cyclin A2 activates the RhoA–ROCK pathway through a direct interaction with RhoA that, contrary to Cyclin D1, requires neither its Cdk-interacting domain nor p27 because it is efficient both in *Cdk2*$^{-/-}$ cells treated by a Cdk1 inhibitor and in *p27*$^{-/-}$ cells (Fig. 3 and Fig. S3, E and F). This is consistent with the rescue of the cortical Actin phenotype by a mutant Cyclin A2 unable to bind Cdk1 and Cdk2. Furthermore, this is dependent on its cytoplasmic localization because targeting the mutant to the nucleus prevents rescue. Although an initial study indicated that Cyclin A2 is exclusively nuclear, it was demonstrated that Cyclin A2 continuously shuttles between the nucleus and the

cytoplasm, where nuclear import requires association with Cdk2 (Jackman et al., 2002). A subsequent study further confirmed Cyclin A2 cytoplasmic localization, where it is trapped in a complex with Cdk2 at the endoplasmic reticulum by SCAPER (Tsang et al., 2007).

It is interesting that Cyclin D1 and Cyclin A2 act in an opposite way on RhoA activation. Moreover, Rho family GTPases are integral components of signaling pathways that control the transcription of cell cycle effectors induced by external cues, such as growth factors or cell adhesion to the extracellular matrix (Philips et al., 2000; Teramoto et al., 2003; Croft and Olson, 2006). These data illustrate the intricate cross talk between Cyclins, Cdk inhibitor expression, and Rho family GTPase activity.

Our results add another component to the complex regulatory network that involves cell cycle regulators and cytoskeletal structures that participate in the control of cell movement. Interestingly, depletion of Cyclin A2 is sufficient to increase cell motility in 2D assays and cooperates with oncogenic transformation to increase invasiveness in 3D collagen matrixes. Accordingly, Cyclin A2 protein levels are significantly lower in a more invasive colon carcinoma cell line and, more importantly, in metastases versus primary colon adenocarcinoma. Our data from cultured cell lines indicate that its down-regulation is an important component in the complicated process of metastasis and, thereby, suggest its utility as a prognostic indicator. This concurs with studies on renal, colorectal carcinoma, and prostate cancer, which found that tumors with a large proportion of proliferating cells that show low levels of Cyclin A2 protein were more aggressive than those with high Cyclin A2 expression (Mashal et al., 1996; Aaltomaa et al., 1999; Davidson et al., 2001; Li et al., 2002; Migita et al., 2002; Bondi et al., 2005). Moreover, although Nm23-H1 is the primary prognostic indicator for oral squamous cell carcinoma metastasis to lymph nodes, Cyclin A2 levels were inversely correlated to invasiveness of oral squamous cell carcinoma both in vitro and in vivo (Wang et al., 2008).

Collectively, these observations shed new light on the role of Cyclin A2 in cancer and metastases. Cyclin A2 is frequently overexpressed in highly proliferative cancers and, as such, has been considered as a proliferation marker. In fact, we would argue that its misregulated expression in cancer could give rise to distinct phenotypes, depending on both the level and subcellular localization of the protein.

Materials and methods

Plasmids

Mouse Cyclin A2 cDNA was cloned into pBluescript II KS (Agilent Technologies). Site-directed mutagenesis was performed using a mutagenesis kit (QuikChange II; Agilent Technologies). Cyclin A2 mutants were obtained by substitutions of the indicated amino acid residues by alanine. The different Cyclin A2 constructs were additionally mutated to be resistant to the shRNA used and subcloned into pcDNA3 (Invitrogen). Sequences were fused to a 3×Flag tag at their 3′ end. Optionally, the SV40 large T antigen NLS and the MEK1 NES were inserted between the Cyclin A2 cDNA and the Flag tag. WT Cyclin A2–Flag and mutated cDNAs were introduced into pMSCVhyg (Takara Bio Inc.) for retrovirus production. Cyclin A2 cDNA, N-terminal Cyclin A2 (coding for amino acids 1–196), and C-terminal Cyclin A2 (coding for amino acids 196–422) fragments and mouse Cyclin E1 were also subcloned into pGEX-6P-1 (GE Healthcare).

shRNA a–e directed against Cyclin A2 mRNA were tested. The most efficient, shRNA a and b, were both used for all experiments with the exception of the depletion in MDA-MB-231 in which only shRNA b, which targets the mouse and human Cyclin A2 sequence, was used: shRNA a, 5′-GAAATGGAGGTTAAATGA-3′; shRNA b, 5′-GTAGCAGAGTTTGTGTATA-3′; shRNA c, 5′-GGAGGTTAAATGTAAACCTA-3′; shRNA d, 5′-CTTAGGGAAATGGAGGTTA-3′; and shRNA e, 5′-GGCCAGGATGCTCTAATTCT-3′. They were cloned into the RNAi-Ready pSIREN-RetroQ vector (Takara Bio Inc.).

Plasmids containing mouse RhoAWT, N19, and V14 mutant fused to EGFP were gifts from C. Gauthier-Rouvière (Centre de Recherche de Biochimie Macromoléculaire, Montpellier, France). Plasmids encoding RhoB and RhoC fused to EGFP were gifts from C.J. Der (University of North Carolina at Chapel Hill, Chapel Hill, NC; Roberts et al., 2008). RhoA cDNA was subcloned into pGEX-2T (GE Healthcare).

Cell culture, transfections, and infections

NIH3T3 cells, primary human skin fibroblasts, and immortalized *Cdk2*$^{-/-}$ mouse fibroblasts were gifts from M.-L. Vignais (Institut des Neurosciences, Montpellier, France) and M. Barbacid (Centro Nacional de Investigaciones Oncológicas, Madrid, Spain). Cells were maintained in DME medium with 10% FCS. NIH3T3-RasV12, SW480, SW620, and MDA-MB-231 cells were gifts from P. Roux (Centre de Recherche de Biochimie Macromoléculaire, Montpellier, France) and cultivated in DME (NIH3T3-RasV12), RPMI 1640 (SW480 and SW620), or MEM (MDA-MB-231) medium supplemented with 10% FCS. Cells were synchronized after confluence for 24 h and, when required, treated for 24 h with RO 3306 (EMD) Cdk1 inhibitor at 10 µM.

Transfections were performed using Lipofectamine 2000 (Invitrogen). After virus infection, cells were selected for 2 d in the presence of 1–10 µg/ml puromycin (InvivoGen), depending on cell lines, or 200–250 µg/ml hygromycin B (Invitrogen).

Growth assays, quantification of cell dimensions, and FACS

For growth assays, NIH3T3 cells infected with shCycA2- and shLuc-coding viruses were selected for 2 d and seeded at a density of 10^4 cells/35-mm plate without antibiotic. Cells were counted in triplicates everyday for 7 d. Quantification of cell dimensions (diameter and volume) were performed in triplicates using a CASY 1 device (Schafe System).

For cell cycle analysis, after synchronization, cells were cultivated for 24 h and then fixed in 90% cold ethanol, washed in PBS, and labeled overnight using 4 µg/ml 7AAD. They were analyzed by flow cytometry on a flow cytometer (FACScan; BD) with CellQuest software (BD; Coisy-Quivy et al., 2006).

Antibodies, immunoblotting, and immunofluorescence

The following antibodies were used for immunoblotting: monoclonal (clone CY-A1; Sigma-Aldrich) and polyclonal anti–Cyclin A2 (sc-751; Santa Cruz Biotechnology, Inc.), anti-Flag (M2; Sigma-Aldrich), anti-Cdk2 (sc-163; Santa Cruz Biotechnology, Inc.), anti-Cdk1 (mouse monoclonal; BD), anti-p107 (sc-318; Santa Cruz Biotechnology, Inc.), anti-p21 (sc-397-G; Santa Cruz Biotechnology, Inc.), anti-p27 (sc-528-G; Santa Cruz Biotechnology, Inc.), anti-RhoA (sc-418; Santa Cruz Biotechnology, Inc.), anti-RhoC (clone D40E4; Cell Signaling Technology), anti-RhoB (sc-180; Santa Cruz Biotechnology, Inc.), anti-Rac1 (clone 102; BD), anti-Cofilin (ACFL02-A; Cytoskeleton), anti–P-Ser3 Cofilin (sc-12912-R; Santa Cruz Biotechnology, Inc.), and anti-GAPDH (G9545; Sigma-Aldrich). Secondary HRP-conjugated antibodies were obtained from Thermo Fisher Scientific.

The following antibodies were used for immunofluorescence staining: monoclonal anti-Vinculin (clone hVIN; Sigma-Aldrich) and monoclonal anti-Flag. Staining of F-Actin was performed using phalloidin conjugated with rhodamine (Sigma-Aldrich). Secondary antibodies were Alexa Fluor conjugates (Invitrogen). Before immunofluorescence analysis, cells were fixed with 3.2% paraformaldehyde and permeabilized with 0.2% Triton X-100 (Coisy et al., 2004). Cells were visualized using microscopes (DMRA or DM6000; Leica) and MetaMorph software (Molecular Devices). For immunohistochemistry, anti–human Cyclin A2 (NCL-Cyclin A2; Novocastra) was used.

Coimmunoprecipitation, kinase assay, and GST pull-down

Immunoprecipitations were performed using anti-Flag M2 affinity gel (Sigma-Aldrich) or GFP-Trap beads (ChromoTek) in NP-40 lysis buffer (150 mM NaCl, 1 mM EDTA, 50 mM Hepes, pH 7.9, and 0.5% NP-40). After washes, beads were either resuspended in Laemmli buffer for Western blot analysis or washed additionally with reaction buffer (20 mM Tris, pH 7.5,

and 7.5 mM $MgCl_2$) for kinase assays. The final pellet was resuspended in 25 µl kinase buffer supplemented with 50 µl ATP 0.2 mM, 500 µmol/liter DTT, 4 µg histone H1, and 2.5 µCi γ-[^{32}P]ATP. After incubation for 30 min at 37°C, the reaction was stopped by the addition of Laemmli sample buffer and heating for 10 min at 37°C (Coisy-Quivy et al., 2006).

In vitro binding assays were performed with bacterially produced GST-fused Cyclin A2 and RhoA purified on glutathione-conjugated agarose beads (Thermo Fisher Scientific) according to standard methods (Debant et al., 1996; Lu and Settleman, 1999; Newsome et al., 2000). Recombinant Cyclin A2 was released from beads by digestion using protease (PreScission; GE Healthcare). GST-RhoAWT (10 µg/assay) was incubated at 30°C for 30 min in 100 µl nucleotide exchange buffer (50 mM Tris-Cl, pH 7.5, 5 mM EDTA, 50 mM NaCl, 0.1 mM DTT, and 0.5 mg/ml BSA) with 0.5 mM GDP or 0.5 mM GTPγS (to generate GST-RhoA-GDP or GST-RhoA-GTP forms) or without any nucleotide (for the nucleotide-free GST-RhoA form). The reaction was stopped by adding $MgCl_2$ (final concentration of 20 mM). Cyclin A2 recombinant protein was incubated with GST-RhoAWT (nucleotide-free; GDP or GTPγS bound) or GST beads at 4°C for 15 min. Beads were washed three times in nucleotide exchange buffer supplemented with 20 mM $MgCl_2$. RhoA-GST beads and control beads were then subjected to Western blot analysis.

Adhesion, migration, and invasion assays

Adhesion was monitored 30 min after seeding cells (7×10^3) in 35-mm culture dishes. Wound-healing migration was assayed on confluent cells and monitored using time-lapse microscopy. Data acquisitions were performed every 5 min on a mean of 24-h time course using multisite microscopy as described in the next paragraph. Videos were analyzed using ImageJ (National Institutes of Health), and quantifications were performed with Photoshop (Adobe) software.

For Boyden chamber migration assays, 8-µm pore inserts (BD) were used. Cells in the upper chamber were resuspended in DME–1% FCS, whereas the lower chamber was filled with DME–10% FCS. After 5 h, cells adherent to the lower side of the insert were fixed, stained using crystal violet, and counted. Data are expressed as mean numbers for at least six imaging fields.

Invasion assays were performed in 96-well dishes (PerkinElmer) coated with 0.2% BSA (Sigma-Aldrich) and 10^4 red fluorescent polystyrene microspheres (FluoSpheres; Invitrogen; Smith et al., 2008). In brief, cells were suspended in 2.3 mg/ml serum-free liquid bovine collagen at 10^5 cells/ml. 100-µl aliquots were dispensed into the plates. Plates were centrifuged at 1,000 rpm and incubated in a 37°C/5% CO_2 tissue-culture incubator. Once collagen had polymerized, FCS was added on top of the collagen to a final concentration of 5% for MDA-MB-231 cells and 3% for NIH3T3-RasV12 (final volume of 30 µl). After 48 h for NIH3T3-RasV12 and 24 h for MDA-MB-231, cells were fixed with 4% formaldehyde (final concentration) and stained with 2 µg/ml Hoechst H-1399 (Invitrogen). Confocal z slices were collected from each well at 50 and 0 µm from the bottom of the well. The invasion index was calculated as the ratio of cells at 50:0 µm.

Imaging and fluorescence analysis

Fixed cells were viewed using a microscope (AxioImager Z1; Carl Zeiss) with 63× Plan Apochromat 1.4 NA oil lenses (Carl Zeiss). Images were collected using a charge-coupled device camera (CoolSNAP HD2; Roper Scientific) driven by MetaMorph 7.1 software. For time-lapse experiments, cells (37°C heated and humidified chamber) were viewed using an inverted microscope (Axiovert 200M; Carl Zeiss) with 10× Plan Neofluar 0.3 NA. Images were collected using a camera (Micromax YHS 13001; Roper Scientific) monitored by MetaMorph Software. Cell invasion was monitored using a live inverted microscope (ArrayScan VTI; Thermo Fisher Scientific), and the nuclear staining was quantified with Cellomics software (Thermo Fisher Scientific).

Pull-down of active Rho GTPases and binding assays

Cells were lysed in buffer supplemented with protease inhibitor and incubated for 1 h at 4°C, either with 60 µg Rhotekin–Rho-binding domain protein GST beads (Cytoskeleton) for RhoA and RhoC or 20 µg p21-activated kinase–GST protein beads (Cytoskeleton) for Rac1 pull-down (Borm et al., 2005).

After SDS-PAGE and Western blotting using anti-RhoA, anti-RhoC, and Rac1 antibodies, GTPase activation was evaluated by measuring bands intensities with ImageJ software. The activation index was calculated as pull-down/input/GAPDH intensity ratio.

In vitro exchange assays

Recombinant RhoA was preincubated with full-length Cyclin A2, N-terminal Cyclin A2, C-terminal Cyclin A2, or irrelevant recombinant proteins (MBP, GST, or Cyclin E1) at equimolar concentration (1 µM) for 15 min on ice. Preincubated proteins were added to loading buffer (20 mM Tris-Cl, pH 7.5, 50 mM NaCl, 2 mM $MgCl_2$, 1 mM DTT, and 50 mg/ml BSA) containing 1 µM Mant-GTP (Invitrogen) and 0.4 µM Tgat or 0.5 µM Dbl. Fluorescence measurements were performed using a microplate fluorescence reader (FLx800; BioTek Instruments, Inc.) and KC4 software (BioTek Instruments, Inc.) every 10 s for 10 min at 25°C, monitoring the relative Mant fluorescence (λ-excitation = 360 nm and λ-emission = 460 nm). The initial rate of nucleotide exchange was calculated by linear regression of the fluorescence intensity curve (Excel software; Microsoft). For each experiment, rates were normalized to the reaction with GEF only. Data are expressed as the mean of three independent experiments.

Selection of human primary and metastatic tumor samples

12 primary colorectal cancers were selected with their related metastases: eight hepatic, one rectal, one from the small intestine, one from a lymph node, and one from the peritoneum. The primary consisted of 10 colon cancers and two rectal cancers. All the tumors were conventional adenocarcinomas that were classified according to the seventh TNM (tumor, node, metastase) classification of malignant tumors. All primaries were associated with positive regional lymph nodes: three were pT3N0, three were pT3N1, one was pT3N2, one was pT4bN0, two were pT4N1, one was pT4bN2, and one was pT2N1. Overall, 10 primaries were associated with synchronous metastases and were initially classified as stage IV: two had metachronous metastases, with two initially classified as stage III and II. Among the patients, six received preoperative chemotherapy. Frozen tumor sections were performed before protein extraction, and only samples having >50% of tumor tissue were selected for further analyses. Our local research board approved the study.

For detection of Cyclin A2 protein levels by Western blotting, frozen sections of tumor samples were homogenized in extraction buffer (150 mM NaCl, 10 mM Tris, pH 7.4, 1 mM EDTA, 1 mM EGTA, 1% Triton X-100, and 0.5% NP-40 completed with protease inhibitors) for 20 s at 4,000 Hz using a lyser (MagNA; Roche). After incubation on ice (30 min), samples were centrifuged for 30 min at 14,000 rpm to clear protein lysate from aggregates and lipids. For each sample, 20 µg of total protein extract was analyzed by Western blotting.

Immunohistochemistry

Paraffin-embedded tissue microarrays of colorectal primary tumors, metastases, and normal tissues were obtained from SuperBioChips. The tumors were classified as adenocarcinomas according to the seventh TNM classification of malignant tumors: four were pT3N1, three were pT3N2, and one was pT3N0. Among them, seven were classified as stage IV, and one was classified as stage III.

For the labeling, anti–Cyclin A2 antibody was used after antigen retrieval in citrate buffer and according to standard procedures. Slides were scanned using virtual microscopy (Nanozoomer; Hamamatsu Photonics).

Statistical analysis

Data are reported as arithmetic means ± SEM. Statistical analyses were performed using nonparametric Mann–Whitney test performed with Prism software (GraphPad Software). Statistical significance was defined as $P \leq 0.05$.

Online supplemental material

Fig. S1 shows that depletion of Cyclin A2 in NIH3T3 cells induces changes of several parameters. Fig. S2 shows that Cyclin A2 depletion affects cell size and morphology. Fig. S3 shows that depletion of Cyclin A2 in primary human skin fibroblasts, U2OS cells, and in $p27^{-/-}$ mouse embryonic fibroblasts induces Actin cytoskeleton and adhesion plaque rearrangements as in mouse NIH3T3 cells. Fig. S4 shows Cyclin A2 interaction with different RhoA isoforms, RhoB, and RhoC. Fig. S5 shows that reintroduction of WT or mutant Cyclin A2 upon depletion of Cyclin A2 reduces migration ability of NIH3T3 cells to the level of the WT. Video 1, related to Fig. 7, shows migration of NIH3T3 cells infected with shLuc retrovirus in a wound-healing assay. Video 2, related to Fig. 7, shows migration of NIH3T3 cells infected with shCycA2 retrovirus in a wound-healing assay. Online supplemental material is available at http://www.jcb.org/cgi/content/full/jcb.201102085/DC1.

This work was made possible thanks to the Montpellier RIO (research interorganism) Imaging facility. We thank Thierry Gostan for his help with statistical analysis and Rachel Audo and Patricia Cavelier for their help with the immunohistochemistry analysis. We are grateful to Robert Hipskind, Claude Sardet, Pierre Roux, Anne Debant, Susanne Schmidt, Dominique Joubert, Philippe Jay, and Daniel Fisher for their helpful discussions and comments on our manuscript.

This work and N. Arsic were supported by grants from Agence Nationale de la Recherche (BLANC06-3_142605), the Marie Curie reintegration program (MIRG-CT-2006-044922), and Association pour la Recherche contre le Cancer. N. Bendris was supported by a fellowship from the French Ministry of Education and Research and Fondation pour la Recherche Médicale.

Submitted: 16 February 2011
Accepted: 7 December 2011

References

Aaltomaa, S., P. Lipponen, M. Ala-Opas, M. Eskelinen, K. Syrjänen, and V.M. Kosma. 1999. Expression of cyclins A and D and p21(waf1/cip1) proteins in renal cell cancer and their relation to clinicopathological variables and patient survival. *Br. J. Cancer*. 80:2001–2007. http://dx.doi.org/10.1038/sj.bjc.6690634

Bergmann-Leitner, E.S., and S.I. Abrams. 2000. Differential role of Fas/Fas ligand interactions in cytolysis of primary and metastatic colon carcinoma cell lines by human antigen-specific CD8+ CTL. *J. Immunol.* 164:4941–4954.

Besson, A., M. Gurian-West, A. Schmidt, A. Hall, and J.M. Roberts. 2004. p27Kip1 modulates cell migration through the regulation of RhoA activation. *Genes Dev.* 18:862–876. http://dx.doi.org/10.1101/gad.1185504

Bondi, J., A. Husdal, G. Bukholm, J.M. Nesland, A. Bakka, and I.R. Bukholm. 2005. Expression and gene amplification of primary (A, B1, D1, D3, and E) and secondary (C and H) cyclins in colon adenocarcinomas and correlation with patient outcome. *J. Clin. Pathol.* 58:509–514. http://dx.doi.org/10.1136/jcp.2004.020347

Borm, B., R.P. Requardt, V. Herzog, and G. Kirfel. 2005. Membrane ruffles in cell migration: indicators of inefficient lamellipodia adhesion and compartments of actin filament reorganization. *Exp. Cell Res.* 302:83–95. http://dx.doi.org/10.1016/j.yexcr.2004.08.034

Bos, J.L., H. Rehmann, and A. Wittinghofer. 2007. GEFs and GAPs: critical elements in the control of small G proteins. *Cell*. 129:865–877. http://dx.doi.org/10.1016/j.cell.2007.05.018

Burridge, K., and K. Wennerberg. 2004. Rho and Rac take center stage. *Cell*. 116:167–179. http://dx.doi.org/10.1016/S0092-8674(04)00003-0

Coisy, M., V. Roure, M. Ribot, A. Philips, C. Muchardt, J.M. Blanchard, and J.C. Dantonel. 2004. Cyclin A repression in quiescent cells is associated with chromatin remodeling of its promoter and requires Brahma/SNF2alpha. *Mol. Cell*. 15:43–56. http://dx.doi.org/10.1016/j.molcel.2004.06.022

Coisy-Quivy, M., O. Disson, V. Roure, C. Muchardt, J.M. Blanchard, and J.C. Dantonel. 2006. Role for Brm in cell growth control. *Cancer Res.* 66:5069–5076. http://dx.doi.org/10.1158/0008-5472.CAN-05-0596

Croft, D.R., and M.F. Olson. 2006. The Rho GTPase effector ROCK regulates cyclin A, cyclin D1, and p27Kip1 levels by distinct mechanisms. *Mol. Cell. Biol.* 26:4612–4627. http://dx.doi.org/10.1128/MCB.02061-05

Davidson, B., B. Risberg, A. Berner, J.M. Nesland, C.G. Tropé, G.B. Kristensen, M. Bryne, M. Goscinski, G. van de Putte, and V.A. Flørenes. 2001. Expression of cell cycle proteins in ovarian carcinoma cells in serous effusions-biological and prognostic implications. *Gynecol. Oncol.* 83:249–256. http://dx.doi.org/10.1006/gyno.2001.6388

Debant, A., C. Serra-Pagès, K. Seipel, S. O'Brien, M. Tang, S.H. Park, and M. Streuli. 1996. The multidomain protein Trio binds the LAR transmembrane tyrosine phosphatase, contains a protein kinase domain, and has separate rac-specific and rho-specific guanine nucleotide exchange factor domains. *Proc. Natl. Acad. Sci. USA*. 93:5466–5471. http://dx.doi.org/10.1073/pnas.93.11.5466

De Boer, L., V. Oakes, H. Beamish, N. Giles, F. Stevens, M. Somodevilla-Torres, C. Desouza, and B. Gabrielli. 2008. Cyclin A/cdk2 coordinates centrosomal and nuclear mitotic events. *Oncogene*. 27:4261–4268. http://dx.doi.org/10.1038/onc.2008.74

Etienne-Manneville, S., and A. Hall. 2002. Rho GTPases in cell biology. *Nature*. 420:629–635. http://dx.doi.org/10.1038/nature01148

Fung, T.K., H.T. Ma, and R.Y. Poon. 2007. Specialized roles of the two mitotic cyclins in somatic cells: cyclin A as an activator of M phase-promoting factor. *Mol. Biol. Cell*. 18:1861–1873. http://dx.doi.org/10.1091/mbc.E06-12-1092

Geisen, C., and T. Moroy. 2002. The oncogenic activity of cyclin E is not confined to Cdk2 activation alone but relies on several other, distinct functions of the protein. *J. Biol. Chem.* 277:39909–39918. http://dx.doi.org/10.1074/jbc.M205919200

Geng, Y., Y.M. Lee, M. Welcker, J. Swanger, A. Zagozdzon, J.D. Winer, J.M. Roberts, P. Kaldis, B.E. Clurman, and P. Sicinski. 2007. Kinase-independent function of cyclin E. *Mol. Cell*. 25:127–139. http://dx.doi.org/10.1016/j.molcel.2006.11.029

Goda, T., M. Funakoshi, H. Suhara, T. Nishimoto, and H. Kobayashi. 2001. The N-terminal helix of *Xenopus* cyclins A and B contributes to binding specificity of the cyclin-CDK complex. *J. Biol. Chem.* 276:15415–15422. http://dx.doi.org/10.1074/jbc.M011101200

Hayashi, S., and M. Yamaguchi. 1999. Kinase-independent activity of Cdc2/cyclin A prevents the S phase in the *Drosophila* cell cycle. *Genes Cells*. 4:111–122. http://dx.doi.org/10.1046/j.1365-2443.1999.00243.x

Heasman, S.J., and A.J. Ridley. 2008. Mammalian Rho GTPases: new insights into their functions from in vivo studies. *Nat. Rev. Mol. Cell Biol.* 9:690–701. http://dx.doi.org/10.1038/nrm2476

Jackman, M., Y. Kubota, N. den Elzen, A. Hagting, and J. Pines. 2002. Cyclin A- and cyclin E-Cdk complexes shuttle between the nucleus and the cytoplasm. *Mol. Biol. Cell*. 13:1030–1045. http://dx.doi.org/10.1091/mbc.01-07-0361

Jirawatnotai, S., Y. Hu, W. Michowski, J.E. Elias, L. Becks, F. Bienvenu, A. Zagozdzon, T. Goswami, Y.E. Wang, A.B. Clark, et al. 2011. A function for cyclin D1 in DNA repair uncovered by protein interactome analyses in human cancers. *Nature*. 474:230–234. http://dx.doi.org/10.1038/nature10155

Kalaszczynska, I., Y. Geng, T. Iino, S. Mizuno, Y. Choi, I. Kondratiuk, D.P. Silver, D.J. Wolgemuth, K. Akashi, and P. Sicinski. 2009. Cyclin A is redundant in fibroblasts but essential in hematopoietic and embryonic stem cells. *Cell*. 138:352–365. http://dx.doi.org/10.1016/j.cell.2009.04.062

Lamb, J., S. Ramaswamy, H.L. Ford, B. Contreras, R.V. Martinez, F.S. Kittrell, C.A. Zahnow, N. Patterson, T.R. Golub, and M.E. Ewen. 2003. A mechanism of cyclin D1 action encoded in the patterns of gene expression in human cancer. *Cell*. 114:323–334. http://dx.doi.org/10.1016/S0092-8674(03)00570-1

Leibovitz, A., J.C. Stinson, W.B. McCombs III, C.E. McCoy, K.C. Mazur, and N.D. Mabry. 1976. Classification of human colorectal adenocarcinoma cell lines. *Cancer Res.* 36:4562–4569.

Li, J.Q., H. Miki, F. Wu, K. Saoo, M. Nishioka, M. Ohmori, and K. Imaida. 2002. Cyclin A correlates with carcinogenesis and metastasis, and p27(kip1) correlates with lymphatic invasion, in colorectal neoplasms. *Hum. Pathol.* 33:1006–1015. http://dx.doi.org/10.1053/hupa.2002.125774

Li, Z., X. Jiao, C. Wang, X. Ju, Y. Lu, L. Yuan, M.P. Lisanti, S. Katiyar, and R.G. Pestell. 2006a. Cyclin D1 induction of cellular migration requires p27(KIP1). *Cancer Res.* 66:9986–9994. http://dx.doi.org/10.1158/0008-5472.CAN-06-1596

Li, Z., C. Wang, X. Jiao, Y. Lu, M. Fu, A.A. Quong, C. Dye, J. Yang, M. Dai, X. Ju, et al. 2006b. Cyclin D1 regulates cellular migration through the inhibition of thrombospondin 1 and ROCK signaling. *Mol. Cell. Biol.* 26:4240–4256. http://dx.doi.org/10.1128/MCB.02124-05

Li, Z., C. Wang, G.C. Prendergast, and R.G. Pestell. 2006c. Cyclin D1 functions in cell migration. *Cell Cycle*. 5:2440–2442. http://dx.doi.org/10.4161/cc.5.21.3428

Lu, Y., and J. Settleman. 1999. The *Drosophila* Pkn protein kinase is a Rho/Rac effector target required for dorsal closure during embryogenesis. *Genes Dev.* 13:1168–1180. http://dx.doi.org/10.1101/gad.13.9.1168

Martín, A., J. Odajima, S.L. Hunt, P. Dubus, S. Ortega, M. Malumbres, and M. Barbacid. 2005. Cdk2 is dispensable for cell cycle inhibition and tumor suppression mediated by p27(Kip1) and p21(Cip1). *Cancer Cell*. 7:591–598. http://dx.doi.org/10.1016/j.ccr.2005.05.006

Mashal, R.D., S. Lester, C. Corless, J.P. Richie, R. Chandra, K.J. Propert, and A. Dutta. 1996. Expression of cell cycle-regulated proteins in prostate cancer. *Cancer Res.* 56:4159–4163.

McAllister, S.S., M. Becker-Hapak, G. Pintucci, M. Pagano, and S.F. Dowdy. 2003. Novel p27(kip1) C-terminal scatter domain mediates Rac-dependent cell migration independent of cell cycle arrest functions. *Mol. Cell. Biol.* 23:216–228. http://dx.doi.org/10.1128/MCB.23.1.216-228.2003

Migita, T., Y. Oda, S. Naito, and M. Tsuneyoshi. 2002. Low expression of p27(Kip1) is associated with tumor size and poor prognosis in patients with renal cell carcinoma. *Cancer*. 94:973–979. http://dx.doi.org/10.1002/cncr.10338

Morgan, D.O. 1997. Cyclin-dependent kinases: engines, clocks, and microprocessors. *Annu. Rev. Cell Dev. Biol.* 13:261–291. http://dx.doi.org/10.1146/annurev.cellbio.13.1.261

Moriyama, K., and I. Yahara. 1999. Two activities of cofilin, severing and accelerating directional depolymerization of actin filaments, are affected differentially by mutations around the actin-binding helix. *EMBO J.* 18:6752–6761. http://dx.doi.org/10.1093/emboj/18.23.6752

Murphy, M., M.G. Stinnakre, C. Senamaud-Beaufort, N.J. Winston, C. Sweeney, M. Kubelka, M. Carrington, C. Bréchot, and J. Sobczak-Thépot. 1997. Delayed early embryonic lethality following disruption of the murine cyclin A2 gene. *Nat. Genet.* 15:83–86. http://dx.doi.org/10.1038/ng0197-83

Newsome, T.P., S. Schmidt, G. Dietzl, K. Keleman, B. Asling, A. Debant, and B.J. Dickson. 2000. Trio combines with dock to regulate Pak activity

during photoreceptor axon pathfinding in *Drosophila*. *Cell*. 101:283–294. http://dx.doi.org/10.1016/S0092-8674(00)80838-7

Nigg, E.A. 1995. Cyclin-dependent protein kinases: key regulators of the eukaryotic cell cycle. *Bioessays*. 17:471–480. http://dx.doi.org/10.1002/bies.950170603

Oser, M., and J. Condeelis. 2009. The cofilin activity cycle in lamellipodia and invadopodia. *J. Cell. Biochem.* 108:1252–1262. http://dx.doi.org/10.1002/jcb.22372

Pagano, M., R. Pepperkok, F. Verde, W. Ansorge, and G. Draetta. 1992. Cyclin A is required at two points in the human cell cycle. *EMBO J.* 11:961–971.

Philips, A., P. Roux, V. Coulon, J.M. Bellanger, A. Vié, M.L. Vignais, and J.M. Blanchard. 2000. Differential effect of Rac and Cdc42 on p38 kinase activity and cell cycle progression of nonadherent primary mouse fibroblasts. *J. Biol. Chem.* 275:5911–5917. http://dx.doi.org/10.1074/jbc.275.8.5911

Ren, X.D., W.B. Kiosses, D.J. Sieg, C.A. Otey, D.D. Schlaepfer, and M.A. Schwartz. 2000. Focal adhesion kinase suppresses Rho activity to promote focal adhesion turnover. *J. Cell Sci.* 113:3673–3678.

Ridley, A.J., and A. Hall. 1992. The small GTP-binding protein rho regulates the assembly of focal adhesions and actin stress fibers in response to growth factors. *Cell*. 70:389–399. http://dx.doi.org/10.1016/0092-8674(92)90163-7

Ridley, A.J., H.F. Paterson, C.L. Johnston, D. Diekmann, and A. Hall. 1992. The small GTP-binding protein rac regulates growth factor-induced membrane ruffling. *Cell*. 70:401–410. http://dx.doi.org/10.1016/0092-8674(92)90164-8

Roberts, P.J., N. Mitin, P.J. Keller, E.J. Chenette, J.P. Madigan, R.O. Currin, A.D. Cox, O. Wilson, P. Kirschmeier, and C.J. Der. 2008. Rho Family GTPase modification and dependence on CAAX motif-signaled posttranslational modification. *J. Biol. Chem.* 283:25150–25163. http://dx.doi.org/10.1074/jbc.M800882200

Sahai, E., and C.J. Marshall. 2002. RHO-GTPases and cancer. *Nat. Rev. Cancer*. 2:133–142. http://dx.doi.org/10.1038/nrc725

Schmidt, A., and A. Hall. 2002. Guanine nucleotide exchange factors for Rho GTPases: turning on the switch. *Genes Dev.* 16:1587–1609. http://dx.doi.org/10.1101/gad.1003302

Schulman, B.A., D.L. Lindstrom, and E. Harlow. 1998. Substrate recruitment to cyclin-dependent kinase 2 by a multipurpose docking site on cyclin A. *Proc. Natl. Acad. Sci. USA*. 95:10453–10458. http://dx.doi.org/10.1073/pnas.95.18.10453

Smith, H.W., P. Marra, and C.J. Marshall. 2008. uPAR promotes formation of the p130Cas–Crk complex to activate Rac through DOCK180. *J. Cell Biol.* 182:777–790. http://dx.doi.org/10.1083/jcb.200712050

Tanaka, H., T. Yamashita, M. Asada, S. Mizutani, H. Yoshikawa, and M. Tohyama. 2002. Cytoplasmic $p21^{Cip1/WAF1}$ regulates neurite remodeling by inhibiting Rho-kinase activity. *J. Cell Biol.* 158:321–329. http://dx.doi.org/10.1083/jcb.200202071

Teramoto, H., R.L. Malek, B. Behbahani, M.D. Castellone, N.H. Lee, and J.S. Gutkind. 2003. Identification of H-Ras, RhoA, Rac1 and Cdc42 responsive genes. *Oncogene*. 22:2689–2697. http://dx.doi.org/10.1038/sj.onc.1206364

Tsang, W.Y., L. Wang, Z. Chen, I. Sánchez, and B.D. Dynlacht. 2007. SCAPER, a novel cyclin A–interacting protein that regulates cell cycle progression. *J. Cell Biol.* 178:621–633. http://dx.doi.org/10.1083/jcb.200701166

Vassilev, L.T. 2006. Cell cycle synchronization at the G2/M phase border by reversible inhibition of CDK1. *Cell Cycle*. 5:2555–2556. http://dx.doi.org/10.4161/cc.5.22.3463

Vega, F.M., and A.J. Ridley. 2008. Rho GTPases in cancer cell biology. *FEBS Lett.* 582:2093–2101. http://dx.doi.org/10.1016/j.febslet.2008.04.039

Vega, F.M., G. Fruhwirth, T. Ng, and A.J. Ridley. 2011. RhoA and RhoC have distinct roles in migration and invasion by acting through different targets. *J. Cell Biol.* 193:655–665. http://dx.doi.org/10.1083/jcb.201011038

Vial, E., E. Sahai, and C.J. Marshall. 2003. ERK-MAPK signaling coordinately regulates activity of Rac1 and RhoA for tumor cell motility. *Cancer Cell*. 4:67–79. http://dx.doi.org/10.1016/S1535-6108(03)00162-4

Wang, Y.F., J.Y. Chen, S.Y. Chang, J.H. Chiu, W.Y. Li, P.Y. Chu, S.K. Tai, and L.S. Wang. 2008. Nm23-H1 expression of metastatic tumors in the lymph nodes is a prognostic indicator of oral squamous cell carcinoma. *Int. J. Cancer*. 122:377–386. http://dx.doi.org/10.1002/ijc.23096

Welm, A.L., N.A. Timchenko, Y. Ono, H. Sorimachi, H.S. Radomska, D.G. Tenen, J. Lekstrom-Himes, and G.J. Darlington. 2002. C/EBPalpha is required for proteolytic cleavage of cyclin A by calpain 3 in myeloid precursor cells. *J. Biol. Chem.* 277:33848–33856. http://dx.doi.org/10.1074/jbc.M204096200

Yam, C.H., T.K. Fung, and R.Y. Poon. 2002. Cyclin A in cell cycle control and cancer. *Cell. Mol. Life Sci.* 59:1317–1326. http://dx.doi.org/10.1007/s00018-002-8510-y

Yoshizuka, N., R. Moriuchi, T. Mori, K. Yamada, S. Hasegawa, T. Maeda, T. Shimada, Y. Yamada, S. Kamihira, M. Tomonaga, and S. Katamine. 2004. An alternative transcript derived from the trio locus encodes a guanosine nucleotide exchange factor with mouse cell-transforming potential. *J. Biol. Chem.* 279:43998–44004. http://dx.doi.org/10.1074/jbc.M406082200